GODDARD
GRANT
IN-32-CR

Interim Progress Report on NAG-356

123406

"Optical Communication with Semiconductor Laser Diodes"

F. DAVIDSON

This report covers the period July 1 - December 31, 1987 and takes the form of a manuscript entitled "Slot Clock Recovery in Optical PPM Communication Systems with Avalance Photodiode Photodetectors" which has been submitted to the IEEE Transactions on Communications for publication.

Slot Clock Recovery in Optical PPM Communication Systems with Avalanche Photodiode Photodetectors*

F. Davidson and X. Sun

Dept. of Electrical and Computer Engineering
The Johns Hopkins University
Baltimore, MD 21218

ABSTRACT

Slot timing recovery in a direct detection optical PPM communication system can be achieved by processing the photodetector output waveform with a nonlinear device whose output forms the input to a phase lock loop. The choice of a simple transition detector as the nonlinearity is shown to give satisfactory synchronization performance. The rms phase error of the recovered slot clock and the effect of slot timing jitter on the bit error probability were directly measured. The experimental system consisted of an AlGaAs laser diode (λ=834 nm) and a silicon avalanche photodiode (APD) photodetector and used Q=4 PPM signaling operated at a source data rate of 25 megabits/second. The mathematical model developed to characterize system performance is shown to be in good agreement with the actual performance measurements. The use of the recovered slot clock in the receiver resulted no degradation in receiver sensitivity compared to a system with perfect slot timing. The system achieved a bit error probability of 10^{-6} at received signal energies corresponding to an average of less than 60 detected photons per information bit.

* Work supported by the National Aeronautics and Space Administration

I Introduction

Q-ary pulse position modulation (PPM) signaling is a preferred modulation format in free space direct detection optical communication systems. In this format, a group of L binary source bits are transmitted as a single light pulse positioned in one of $Q=2^L$ possible time slots. The performance of both ideal and nonideal optical communication systems that use PPM signaling has been studied both theoretically and experimentally [1]-[6] under the condition that perfect synchronization of both the time slot boundaries and PPM word boundaries with those of the transmitter is available at the receiver. In practice, some means must be provided for the establishment of this synchronization at the receiver. The actual measured performance of a system that uses a phase lock loop to regenerate the slot clock waveform from the noisy output of a silicon avalanche photodiode (APD) photodetector is reported here. The system used Q=4 PPM signaling to transmit information at a source data rate of 25×10^6 bits/sec. The system was able to maintain slot clock synchronization at bit error probabilities less than 10^{-2}, or at received signal energies that corresponded to more than 30 detected photons per PPM light pulse.

One of the basic problems in any communication system that uses a PPM signaling format is to find a means of establishing both PPM slot and word synchronization between the transmitter and receiver. The optimal receiver for a direct detection PPM optical communication system consists of a device which integrates the APD output signal over each time slot and then compares each of the Q integrated outputs to find the largest. Any offset or jitter in time slot boundaries directly affects the result of the integrations over the time slots, and, consequently, degrades the performance of the entire system. In practice, slot timing synchronization requires a regenerated clock waveform at the receiver at the slot clock frequency and synchronized with the clock at the transmitter. Once the correct slot timing is provided, PPM word synchronization can be established by a properly initialized modulo-Q counter driven by the regenerated slot clock. PPM word synchronization is maintained unless the counter miscounts or the recovered clock jitter is so severe that cycle-slipping occurs. Initial synchronization of the modulo-Q counter is usually done through recognition of a special data pattern transmitted at infrequent intervals. Some recent theoretical studies

of ways to establish PPM word synchronization are given in [7]-[9]. This work addresses only the issues of slot clock synchronization for receivers that use APD photodetectors.

Generally speaking, all the technologies for bit timing extraction in conventional digital telecommunication systems can be used for slot timing recovery in optical PPM communication systems. Modification is necessary, however, to cope with the shot noise of photodetectors that appears with the additive Gaussian noise of subsequent amplifiers. The use of APD's improves detector sensitivity significantly but also introduces so-called excess noise, which is nonadditive and follows the Conradi distribution [10][11]. Several conventional means of timing recovery have been studied for use in optical communications [12]-[17] and some of them are widely used in optical fiber telecommunication systems [18]. Free space optical communication systems, however, are characterized by much higher channel losses, typically 60-70 dB as opposed to 30-35 dB for fiber optic systems.

This paper is organized as follows. The next section gives a brief review of previous studies of slot clock timing recovery for direct detection optical communication systems. Section III discusses transition detector type clock recovery schemes, which are widely used in conventional digital communication systems but have not yet been studied for optical communication systems. A theoretical analysis associated with this system is also developed. This method is easy to implement and was found to be capable of establishing satisfactory slot clock timing recovery. Section IV discusses the effects of slot timing jitter on system performance. Section V describes the experiments and measured performance of this slot timing recovery system. The recovered clock signal at the receiver was sufficient to achieve a bit error probability of 10^{-6} at a detected energy level corresponding to less than 60 detected photons per information bit in our 25×10^6 bits/second laboratory system. No degradation in performance was observed in terms of received bit error probabilities as a function of average number of detected photons per information bit, when compared to the same receiver operated with a common transmitter/receiver slot clock (i.e. perfect receiver slot time synchronization). The theory developed for the design of this type of slot timing recovery system is shown to be appropriate as well.

II Review of Slot Clock Timing Recovery in Direct Detection Optical Communication Systems

The response of an APD to an incident optical field can be modeled as a filtered compound doubly stochastic Poisson process [1, ch. 6] when the amplifier noise is ignored. The basic problem is to estimate slot clock waveforms from the times at which photons are detected from the received optical pulse train. The optimal procedure is to use maximum likelihood (ML) estimation. Under the assumptions that the APD has an unlimited frequency response, the APD output can be modeled as a compound Poisson random point process with intensity function $\lambda(t)$ which is proportional to the intensity of the received optical field. The likelihood function can then be expressed as [1, ch. 3]

$$p[\{N_\sigma;\ t_1 \le \sigma < t_2\} \mid \lambda(t)]$$

$$= \exp\left\{ -\int_{t_1}^{t_2} \lambda(\sigma)d\sigma + \sum_{i=1}^{N_{t_1,t_2}} \ln\lambda(\sigma_i) + \sum_{i=1}^{N_{t_1,t_2}} \ln[P(m_i)] \right\} \qquad (2.1)$$

where $p[\{N_\sigma;\ t_1 \le \sigma < t_2\} \mid \lambda(t)]$ is the sample function density for the occurrence times, the σ_i's, of the photon absorptions, and N_{t_1,t_2} is the total number of photon absorptions within the interval $[t_1,t_2]$. The m_i's are the numbers of secondary electrons generated in the avalanche region of the APD in response to each photon absorption. $P(m_i)$ is given by the Conradi distribution and does not explicitly contain the σ_i.

If the data pattern is known, i.e. $\lambda(t)=\lambda(t-t_0)$ is known except for a time origin t_0, the maximization procedure requires finding t_0 and the set of subsequent pulse boundaries within $[t_1,t_2]$ which maximize (2.1). When the data pattern is not known, the likelihood function is obtained by averaging (2.1) over all possible data patterns. The exact ML estimation scheme usually requires too many computation steps to be carried out in real time. Georghiades [7] derived an approximate likelihood function that reduced the amount of computation significantly and yet gave almost as good synchronization performance as that of the exact likelihood function. A digital computer is still necessary, however, to store the photon absorption times, evaluate the likelihood functions for different time slot boundary shifts, and then find the maximum through comparisons. In

situations where the bandwidth of the APD is limited and the data rate is high, the amplified APD output current cannot be modeled as a point Poisson process, and therefore, the ML synchronization methods described above have to be modified accordingly.

In conventional digital communication systems, a commonly used ML synchronization scheme uses an analog device to compute the derivative of the likelihood function. The result is used to derive an error signal to correct the frequency of the clock oscillator at the receiver [19]. When the data pattern is unknown, an estimated data pattern based on a previously estimated timing base may be used to compute the derivative of the likelihood function. This is referred to as data-added or decision-directed synchronization. The same method was studied for use in optical communication systems by Gagliardi [2]. It was shown that the computation becomes reasonably simple only for a few special pulse shapes, for example, pulses of flat top and exponential rise and fall edges. Rectangular shapes, which are optimal for peak power limited optical transmitters, such as semiconductor laser diodes, are not appropriate for this kind of ML estimation scheme.

A popular variant of ML estimation for rectangular pulses is the early-late gate scheme [20], though it is not mathematically optimal. The early gate integrates the received signal over the first half of the time slot interval and the late gate integrates the signal over the second half of the interval, based on previously estimated time slot boundaries. If the system is perfectly synchronized, the two values of the integrations will be exactly equal on average. Therefore, the difference of the two integrations can be used to derive an error signal to adjust the frequency of the slot clock oscillator. A detailed study of early-late gate synchronization in an optical communication context has been given by Gagliardi [2].

A phase lock loop (PLL) can also be used to regenerate the slot clock at the receiver. Since PPM data streams do not contain a frequency component at the slot clock fundamental frequency, some nonlinearity must be introduced to generate the desired frequency component [21]. Several possible nonlinearities have been studied [15][17], among them are square law, absolute value, ln(cosh) and fourth power. A narrowband filter can also be used to regenerate the slot clock

from such nonlinearly processed PPM waveforms. The use of a PLL can track frequency shifts of the slot clock waveform due to Doppler effects or frequency drift of the transmitter clock oscillator. However, the use of a narrowband filter results in a static phase error given by $\Delta\phi \approx \tan^{-1}(2Q_f\Delta f/f_0)$, where Q_f is the quality factor of the narrowband filter, Δf is the frequency shift, and f_0 is the center frequency of the filter. Andreucci and Mengali [12] have studied timing recovery schemes that use narrowband filters for return-to-zero (RZ) data.

Another class of timing recovery schemes, popular in conventional digital communication systems, are called transition detectors [20]. They generate unipolar output pulses at positive or/and negative going transitions of the input pulses. The power spectrum of the resulting unipolar pulse sequence contains a frequency component at the slot clock fundamental frequency, which can then be tracked by a PLL or a narrowband filter. This method was used in our system and is demonstrated to be a simple, yet very effective means of establishing receiver slot clock synchronization.

III Slot Clock Recovery with a Transition Detector

The shot noise of an APD is signal dependent. Unlike the noise in conventional communication systems, it is neither a stationary nor a Gaussian random process. If the output current of an APD is denoted by $i_A(t)$, the mean square value is given by [22]

$$E\{i_A^2(t)\} = G^2FE\{i_A(t)\} \tag{3.1}$$

where G is the average APD gain, F is the excess noise factor given by $F = k_{eff}G + (2-1/G)(1-k_{eff})$, and k_{eff} is the ratio of ionization coefficients of holes and electrons inside the multiplication region of the APD. The average output current, $E\{i_A(t)\}=e\lambda(t)$ is related to the received optical power as $\lambda(t)=\eta P_0(t)/hf$, where e is the electron charge, η is the quantum efficiency with which received photons are detected and hf is the photon energy. The APD output current is further amplified for processing in the receiver and the amplifier noise, which is stationary and Gaussian, has to be added to the total noise. Usually the APD shot noise dominates when the device is operated at the optimal average gain for which the received bit error probability is minimum. The

amplified APD output signal contains mostly amplitude noise due to the multiplicative nature of the APD shot noise. The transition detector, by intuition, is the least sensitive to amplitude noise of all the commonly used nonlinearities that can be employed to introduce the desired frequency component at the slot clock fundamental frequency in the received PPM waveform. Consequently, it was used rather than one of the other methods in our system.

Figure 1 is a block diagram of this type of system. The input to the system consists of rectangular pulses of width T_s corrupted by signal dependent shot noise and lesser amounts of additive Gaussian noise. The lowpass filter accounts for the limited bandwidth of the APD and the following amplifiers. The threshold crossing detector outputs a triggering pulse to the pulse shaper in response to a positive going transition of an input pulse. The output of the pulse shaper is a rectangular pulse of width $T_s/2$. This choice of pulsewidth maximizes the amplitude of the fundamental frequency component at the slot clock frequency [20]. The pulse shaper has a "dead time" so that it cannot be triggered more than once within one time slot. This prevents false triggering by noise spikes in the APD output current.

The theory of PLL tracking systems has been well developed for conventional communication systems and several studies have been done on optical communication systems as well. It has been shown that for a sufficiently narrow loop bandwidth, the phase error of the regenerate clock waveform has variance given approximately by [15]

$$\sigma_\phi^2 \approx \frac{2B_L N(\omega_s)}{P_s} \tag{3.2}$$

Here $N(\omega)$ is the two sided power spectrum of the noise, ω_s is the angular frequency of the locked PLL, P_s is the power of the sinusoidal component of the input signal at the lock frequency, and B_L is the loop bandwidth given by

$$B_L = \int_0^\infty | H_{PLL}(2\pi f) |^2 df, \tag{3.3}$$

where $H_{PLL}(2\pi f)$ is the transfer function of the linearized model of the PLL.

The phase error of the recovered slot clock obtained with a narrowband filter can also be approximated by (3.2) with the effective loop bandwidth B_L given by [20]

$$B_L = \int_{f_0}^{\infty} | H_{nbf}[2\pi(f - f_0)] |^2 df, \tag{3.4}$$

where $H_{nbf}(2\pi f)$ is the system function of the filter, and f_0 is the center frequency.

Since the input to the PLL is not a stationary random process, the power spectrum can not be obtained by taking the Fourier transform of its autocorrelation function. The alternative is to use the definition given by [21]

$$S(\omega) = \lim_{T\to\infty} \frac{1}{2T} E\{ | X_T(\omega) |^2 \} \tag{3.5}$$

where $X_T(\omega)$ is the Fourier transform of a sample of the signal waveform from -T to T given by

$$X_T(\omega) = \int_{-T}^{T} x(t) e^{-j\omega t} dt \tag{3.6}$$

As in Chen's approach in [15], the input signal to the PLL is defined as

$$x(t) = \sum_n p(t - nQT_s - c_n T_s - \tau_n) \tag{3.7}$$

where p(t) represents the pulse shape, T_s is the duration of a PPM time slot, c_n is an integer from 0 to (Q-1) used to indicate the random PPM pulse position, and τ_n represents random jitter in threshold crossing times. If all transmitted data are equally likely, the c_n' s form a set of independent, identically distributed (i.i.d) random variables. The τ_n' s are also considered to be i.i.d. random variables. Appendix A shows that under these assumptions, the power spectrum (3.5) may be expressed as

$$S(\omega) = | P(\omega) |^2 \left[\frac{1}{QT_s}(1 - | C(\omega) |^2 | M_\tau(\omega) |^2) + \right.$$

$$\left. + \frac{2\pi}{(QT_s)^2} | M_\tau(\omega) |^2 \sum_{k=-\infty}^{\infty} \delta(\omega - 2\pi k/T_s) \right], \tag{3.8}$$

where $P(\omega)$ is the Fourier transform of the pulse shape p(t), $C(\omega)$ and $M_\tau(\omega)$ are the characteristic functions of the c_n and τ_n respectively. These are given by

$$C(\omega) \equiv E\{e^{j\omega T_s c_n}\} = \frac{1}{Q}\sum_{n=0}^{Q-1} e^{j\omega T_s n} \tag{3.9}$$

and

$$M_\tau(\omega) \equiv E\{e^{j\omega\tau_n}\}. \tag{3.10}$$

The first term in (3.8) corresponds to noise and the second term corresponds to the discrete frequency components at the slot clock fundamental frequency and its harmonics. Therefore, the noise power spectrum may be written as

$$N(\omega) = \frac{1}{QT_s} \mid P(\omega) \mid^2 (1 - \mid C(\omega) \mid^2 \mid M_\tau(\omega) \mid^2). \tag{3.11}$$

The total power at the slot clock fundamental frequency is given by

$$P_s = \frac{2}{(QT_s)^2} \mid M_\tau(\omega_s) \mid^2 \mid P(\omega_s) \mid^2. \tag{3.12}$$

If the random jitter represented by the τ_n's can be considered as zero mean Gaussian random variables, then

$$M_\tau(\omega) = e^{-\frac{1}{2}\sigma_\tau^2\omega^2} \tag{3.13}$$

where σ_τ^2 represents the variance of the threshold crossing times which will be determined next.

The input signal to the threshold crossing detector consists of the APD output current, $i_A(t)$, and amplifier thermal noise, $n_t(t)$. The threshold crossing time, t_c, is the solution to the equation $i_A(t_c) + n_t(t_c) = I_{th}$, where I_{th} represents the threshold. The APD output current, $i_A(t)$, can be expressed as the sum of the signal and shot noise, as

$$i_A(t) = s(t) + n_s(t) \tag{3.14}$$

where $s(t) = E\{i_A(t)\}$ and $n_s(t) = i_A(t) - E\{i_A(t)\}$. At high input optical signal levels, the threshold crossing time, t_c, varies within a small region about its mean value T_c. Consequently, it is appropriate to approximate $s(t)$ by the first two terms of its Taylor expansion about T_c, and write

$$I_{th} \approx s(T_c) + s'\ (T_c)(t_c - T_c) + n_s(t_c) + n_t(t_c). \tag{3.15}$$

Since $n_s(t)$ and $n_t(t)$ are independent and $s(T_c)=I_{th}$, it follows that

$$[s'(T_c)]^2\sigma_\tau^2 = E\{n_s^2(t_c)\} + E\{n_t^2(t_c)\}. \tag{3.16}$$

The variance of the amplifier noise is given by

$$E\{n_t^2(t_c)\} = \frac{4kT_rB}{R} \tag{3.17}$$

where k is Boltzmann's constant, T_r is the amplifier equivalent noise temperature, B is the bandwidth of the lowpass filter, and R is the load resistance seen by the APD.

The variance of the shot noise, $E\{n_s^2(t_c)\}$, is equal to the variance of the APD output current, which is a function of t_c. Conditioned on t_c, the APD output current is a filtered compound Poisson process with variance given by [1, ch. 4]

$$E\{n_s^2(t_c) \mid t_c\} = e^2G^2F\int_{-\infty}^{t_c}\lambda(t)h^2(t_c-t)dt. \tag{3.18}$$

where h(t) is the impulse response of the lowpass filter. $\lambda(t)$ is the photon counting intensity function given by

$$\lambda(t) = \begin{cases}\lambda_1 & t\geq t_0\\ \lambda_0 & t<t_0\end{cases} \tag{3.19}$$

where t_0 is the pulse transition time prior to t_c. If the laser has a high on-off extinction ratio and the background radiation appears to be small, i.e. $\lambda_1 >> \lambda_0$,

$$\begin{aligned} E\{n_s^2(t_c) \mid t_c\} &\approx e^2FG^2\lambda_1\int_{t_0}^{t_c}h^2(t_c-t)dt \\ &= e^2FG^2\lambda_1\left[\int_0^{T_c-t_0}h^2(u)du + \int_{T_c-t_0}^{t_c-t_0}h^2(u)du\right]. \end{aligned} \tag{3.20}$$

Since t_c-T_c is very small, the integrand of the second term in (3.20) can be approximated by $h^2(u)\approx h^2(T_c-t_0)+2h(T_c-t_0)\frac{d}{dt}h(T_c-t_0)[u-(T_c-t_0)]$. Averaging both sides of (3.20) over t_c,

$$E\{n_s^2(t_c)\} \approx e^2FG^2\lambda_1\left[\int_0^{T_c-t_0}h^2(u)du + h(T_c-t_0)\frac{d}{dt}h(T_c-t_0)\cdot\sigma_\tau^2\right]. \tag{3.21}$$

Next, according to [1, ch. 4],

$$s(t) = E\{i_A(t)\} = eG \int_{-\infty}^{t} \lambda(u)h(t-u)du \tag{3.22}$$

then

$$s'(t) \approx eG\lambda_1 h(t-t_0) \tag{3.23}$$

where $\lambda_1 >> \lambda_0$ is assumed. Substituting (3.17), (3.21) and (3.23) into (3.16), the variance σ_τ^2 can be solved as

$$\sigma_\tau^2 = \frac{FG^2\lambda_1 \int_0^{T_c-t_0} h^2(u)du + \frac{4kT_rB}{Re^2}}{[G\lambda_1 h(T_c-t_0)]^2 - FG^2\lambda_1 h(T_c-t_0)\frac{d}{dt}h(T_c-t_0)}. \tag{3.24}$$

Equation (3.24) may be evaluated by assuming that the lowpass filter is ideal, i.e.

$$H(j2\pi f) = \begin{cases} e^{-j2\pi f t_d} & |f| \leq B \\ 0 & \text{otherwise'} \end{cases} \tag{3.25}$$

and

$$h(t) = 2B \cdot \frac{\sin 2\pi B(t-t_d)}{2\pi B(t-t_d)} \tag{3.26}$$

where t_d is the time delay of the filter.

There is an optimal point for threshold crossing time T_c, at which (3.24) is minimum. In practice, it corresponds to an optimal threshold level applied to the threshold crossing detector. Figure 2 is a plot of the normalized rms threshold crossing time jitter, σ_τ/T_s, as a function of normalized mean threshold crossing time, $\Delta T_c B$, where $\Delta T_c = T_c-(t_0+t_d)$. In other words, ΔT_c is denoted as the time difference between the mean threshold crossing time, T_c, and the midpoint of the rising edge of the input pulse, t_0+t_d. The curve in figure 2 is nearly flat near $B\Delta T_c = -0.1$. In fact, σ_τ/T_s increases by only 3% when $B\Delta T_c$ changes from its optimal value (≈ -0.08) to zero. Consequently, the value $B\Delta T_c=0$ can be used in (3.24) to a good approximation. This corresponds to a threshold level at one half the peak amplitude of the APD output pulses. As shown in Appendix B, when $B\Delta T_c=0$, (3.24) reduces to

$$\sigma_\tau^2 = \frac{FG^2\lambda_1 + \dfrac{4kT_r}{Re^2}}{4BG^2\lambda_1^2}. \tag{3.27}$$

Finally, substituting (3.27), (3.13), (3.12), (3.11) and (3.9) into (3.2), the variance of the phase error in the recovered slot clock is given by

$$\sigma_\phi^2 = QT_sB_L\cdot\{\exp\left[\frac{\pi^2}{BT_s}\cdot\frac{FG^2\lambda_1T_s + 4kT_rT_s/Re^2}{G^2(\lambda_1T_s)^2}\right] - 1\}. \tag{3.28}$$

The phase error variance, σ_ϕ^2, decreases as the bandwidth of the lowpass filter, B, increases. However, the effect of false triggering by noise spikes is not included in (3.28). This may contribute significantly to the overall phase error when the bandwidth of the lowpass filter becomes too large. In practice, B is also limited by the frequency responses of the APD and the amplifiers. In our experiment, $B=2/T_s$ was used.

IV Effects of Slot Clock Jitter on Probability of Bit Error

Jitter in recovered slot clock timing at the receiver results in the appearance of part of the received PPM pulse energy in an adjacent PPM slot, and hence acts as a source of background noise. If the integrators are ideal, the amount of signal energy which spills over into the adjacent slot is proportional, on average, to the amount of offset in the slot boundaries. If the timing offset of the recovered slot clock is τ, the fractional offset is given by $\epsilon = \tau/T_s$, and the effective average number of signal photons becomes

$$\lambda_1'\ T_s = (1-\epsilon)\lambda_1T_s. \tag{4.1}$$

The effective average number of noise photons in the adjacent slot becomes

$$\lambda_0'\ T_s = \lambda_0T_s + \epsilon\lambda_1T_s. \tag{4.2}$$

The average number of noise photons in the remaining Q-2 time slots is still given by λ_0T_s. The probability of a PPM word error (PWE) is now given by

$$PWE(\epsilon) = 1 - \int_0^\infty P(x \mid \lambda_1'\ T_s)\int_0^x P(y \mid \lambda_0'\ T_s)\left[\int_0^x P(z \mid \lambda_0T_s)dz\right]^{Q-2}dydx \tag{4.3}$$

where $P(u \mid \lambda T_s)$ is the probability density function for the APD output given

that the average number of absorbed photons was $\lambda_1' T_s$, $\lambda_0' T_s$, and $\lambda_0 T_s$ respectively.

Equation (4.3) usually requires excessive computation when evaluated numerically due to the complicated distribution of the APD output. The alternative is to use the union bound as shown below,

$$\mathrm{PWE}(\epsilon) \approx \int_0^\infty P(x \mid \lambda_1' T_s) \int_x^\infty P(y \mid \lambda_0' T_s) dy dx + (Q-2) \int_0^\infty P(x \mid \lambda_1' T_s) \int_x^\infty P(y \mid \lambda_0 T_s) dy dx. \tag{4.4}$$

The union bound gives a good approximation when the input signal to noise ratio is high and the timing offset is small, i.e. $\lambda_1/\lambda_0 >> 1$ and $\epsilon << 1$. A detailed description of an efficient numerical evaluation of (4.4) is given in [6]. The overall probability of a PPM word error is obtained by averaging (4.4) over ϵ. If the timing jitter is assumed to have Gaussian distribution with zero mean and standard deviation given as $\sigma_\epsilon = \sigma_\phi/2\pi$, it follows that

$$\mathrm{PWE} = \int_{-\infty}^{\infty} \mathrm{PWE}(\epsilon) \frac{1}{\sqrt{2\pi}\sigma_\epsilon} e^{-\frac{\epsilon^2}{2\sigma_\epsilon^2}} d\epsilon. \tag{4.5}$$

The probability of bit error (PBE) is given by $\mathrm{PBE} = \frac{Q}{2(Q-1)} \mathrm{PWE}$ [23].

In reality, none of the high speed integration circuits implemented in hardware is ideal and the amount of received signal energy in adjacent slots can not be determined simply by using (4.1) and (4.2). As an example, the integrations over the PPM time slots in our experiment were realized by sampling the output of the tapped delay line matched filter shown in figure 3. Ideally, the impulse response of the matched filter should be a rectangle of width T_s, so that the output in response to a rectangular input pulse is a symmetric triangle of base $2T_s$. A sample at the top of the triangle is proportional to the integration of the energy contained in the input signal within the previous time interval of length T_s. There is no intersymbol interference because the triangle waveform vanishes completely at the next sampling time. However, due to the limited bandwidth of the system, all three corners of the triangle become rounded. If the

input rectangular pulse has zero rise time and fall time, and the lowpass filter has a "brick wall" like frequency response with cutoff frequency $2/T_s$, the output of the matched filter shown in figure 3 can be obtained through Fourier analysis. Figure 4 is a plot of such a distorted triangle along with the associated perfect triangle (dashed line). In practice, input rectangular pulses have finite rise and fall times, and no lowpass filters have true "brick wall" frequency response. It may be impossible to derive the actual distorted triangle shape, and consequently determine the exact amount of received signal energy spilled over into an adjacent slot due to timing offset. When the triangle output by the matched filter becomes rounded, the values of samples at these turning points of the triangle become less sensitive to the sampling times. Therefore, jitter in the recovered slot clock has less effect on the system performance (PWE and PBE) than that when a perfect integrator is used. Nevertheless, (4.5) can be used as an upper bound for the effect of jitter in the recovered slot clock on system performance.

V Measurements of System Performance

A prototype optical communication system was built that consists of a GaAlAs diode laser (Sharp LT024MD, λ=834nm) as the transmitter and a silicon APD (RCA C30902S) as the photodetector. The system used Q=4 PPM signaling at a source data rate of 25 Mbits/second. A detailed description of the system is presented in [5] and [6]. The slot clock recovery system shown in figure 1 was constructed. It used a high speed comparator (Motorola MC1650) as the threshold crossing detector and a monostable multivibrator (Motorola MC10198) as the pulse shaper. The inherent recovery time (dead time) of the multivibrator prevented it from triggering more than once within one slot period. The PLL consisted of a double balanced analog mixer (Motorola MC12002), an active second order loop filter, and a voltage controlled crystal oscillator (VCXO). The effective loop bandwidth was designed and experimentally verified to be about B_L=1 KHz.

Timing errors were measured with the use of an rms phase error detector shown in figure 5. A double-balanced frequency mixer (ASM-15) was used as the phase error detector. Under the conditions of small phase error, the output

voltage can be approximated as $V_{pd}=K_{pd}\Delta\theta$, where K_{pd} is the detector gain, and $\Delta\theta$ is the phase difference between the two input signals. The amplified output of the phase detector was input to an rms to DC converter (Burr-Brown 4341) which had a frequency response from DC to 450 kHz. The output of the phase detector often contained a DC component because a static phase shift between the two input signals was difficult to balance out completely. Since the phase jitter was often very small compared to static phase shifts, a coupling capacitor was inserted between the phase detector output and rms to DC converter input. The coupling capacitor and the input impedance of the rms to DC converter formed a high pass RC filter. A large coupling capacitor was chosen so that the 3dB cutoff frequency was below 0.1 Hz. Two identical slot clock waveforms with a series of known fixed phase shifts were used to calibrate the circuit. It was found that the circuit had a nearly constant gain of 7.62 V/radian for input phase shifts up to $\pm\pi/4$ radians.

Other sources of phase errors that appear in the phase error measurements include noise of circuit components, such as the amplifiers, and the small phase jitter inherent in the VCXO. These phase errors were not included in our model used to compute the phase error, and therefore, should not be included in the measurements. The rms value of these phase errors was determined by feeding the jitter free clock signal into the PLL and then measuring the phase error of the VCXO output against the input jitter free clock. Since the phase jitter of the recovered slot clock is statistically independent of the VCXO noise and other circuit noise, the following relationship holds,

$$\sigma^2_{\phi\text{total}} = \sigma^2_{\phi} + \sigma^2_{\phi\text{n}} \tag{5.1}$$

where $\sigma_{\phi\text{total}}$ is the total measured rms phase error, σ_{ϕ} is the rms phase error of the recovered clock described by (3.28), and $\sigma_{\phi\text{n}}$ accounts for the phase error due to the noises of the VCXO and the circuit. The jitter of the recovered slot clock is then given by

$$\sigma_{\phi} = \sqrt{\sigma^2_{\phi\text{total}} - \sigma^2_{\phi\text{n}}} \approx \sigma_{\phi\text{total}}\left[\,1 - \frac{1}{2}\left(\frac{\sigma_{\phi\text{n}}}{\sigma_{\phi\text{total}}}\right)^2\right] \tag{5.2}$$

Measurements revealed that $\sigma_{\phi\text{n}}$ was about 7.6×10^{-4} radians. The smallest value of $\sigma_{\phi\text{total}}$ measured was about 5×10^{-3}, so that the approximation $\sigma_{\phi} \approx \sigma_{\phi\text{total}}$

was used throughout the measurements.

The optimal level for the threshold crossing detector was set experimentally such that the observed phase error achieved a minimum. As predicted in section III, the optimal threshold was found to be near one half of the average peak amplitude of the APD output pulses, and small deviations from the optimal level resulted in negligible increases in the measured rms phase error. Figure 6 is a plot of the normalized rms phase error of the recovered slot clock, $\sigma_\phi/2\pi$, as a function of the average number of detected photons per information bit given by

$$\text{photons/bit} = \frac{\lambda_1 T_s}{\log_2 Q} = \frac{\eta P_{av} Q T_s}{hf \log_2 Q}. \tag{5.3}$$

Here $\log_2 Q$ is the number of information bits contained in a PPM word, η is the quantum efficiency of the APD, taken to be 77%, and P_{av} is the average optical power incident on the APD. P_{AV} was directly measured by placing an optical power meter at the position of the APD. The measured phase errors of the recovered slot clock using a crystal bandpass filter of effective loop bandwidth B_L=9.5 KHz (full bandwidth 19KHz) is also plotted in figure 6. The solid and dashed curves were obtained from the theoretical analysis. They agreed very well with the measurement data.

Finally, the recovered slot clock was used in the receiver and the system bit error probability was measured as a function of the average number of detected photons per information bit. The data source consisted of pseudo random binary sequences, 1023 bits long. The regenerated binary sequence at the receiver was compared with the properly delayed source binary sequence with the use of an exclusive OR gate. The output of the exclusive OR gate was sampled at the source data rate to form a series of short pulses each of which corresponded to a bit error. A counter was then used to counts the bit errors, and the probability of bit error was obtained by dividing the bit error rate by the source bit rate.

Figure 7 shows the results obtained with the slot clock regenerated by the PLL (B_L=1000Hz) along with the results obtained with the jitter free slot clock (the clock common to the transmitter) at the receiver. The solid curve corresponds to the numerical computations described in [6] that assumed perfect slot timing, and the dotted curve represents the numerical results for the upper

bound given in (4.5) with σ_ϕ determined by (3.28). It is shown that the recovered clock worked so well that no penalty was observed in terms of detected photons per bit at a fixed bit error probability. No cycle slipping and losses of lock were observed until the received optical power dropped below 15 photons per bit (30 photons per pulse) which corresponded to a bit error probability above 0.01. Figure 8 is similar to figure 7 except that the bandpass filter (B_L=9.5KHz) was used in place of the PLL. The dotted curve is again the upper bound given by (4.5) and (3.28). Cycle slipping in this case occurred only when the detected optical power dropped below 30 photons per bit (60 photons per pulse).

Our results for the rms phase errors of the recovered slot clock are comparable with the theoretical results obtained by Chen [15] and Ling [16], which used different methods but did not consider the effect of the APD excess noise and amplifier noise. For example, under the conditions of $B_L T_s = 2.0\times10^{-5}$, 60 signal photons per information bit, and no background radiation, the result in [15] corresponded to $\sigma_\phi/2\pi = 3.5\times10^{-4}$ using a square law device followed by a PLL. The result in [16] with an early-late gate scheme was given by $\sigma_\phi/2\pi = 8.2\times10^{-4}$. Our result under the same conditions was $\sigma_\phi/2\pi = 9.8\times10^{-4}$, which included the effects of the APD shot noise and amplifier noise.

VI Conclusion

We have developed, both in theory and experiment, a transition detector PPM slot clock recovery system. It is easy to implement and gives excellent performance. An upper bound for the probability of bit error with the use of the recovered slot clock in the receiver was derived. The measured performance was shown to be below the upper bound. The limited bandwidth of the matched filter made system performance less sensitive to small amounts of jitter in the times at which the output waveform of the matched filter were sampled.

Appendix A

Power Spectrum of PPM Signal

Substitute (3.7) into (3.6) and let $T=NQT_s$,

$$X_T(\omega) = \sum_{n=-N}^{N} P(\omega)e^{-j\omega(nQT_s+c_nT_s+\tau_n)}. \tag{A.1}$$

Since the c_n's and the τ_n's are two independent sets of i.i.d. random variables,

$$E\{ | X_T(\omega) | ^2\} = | P(\omega) | ^2 \sum_{m,n=-N}^{N} e^{j\omega QT_s(m-n)}E\{e^{j\omega T_s(c_m-c_n)}\}E\{e^{j\omega(\tau_m-\tau_n)}\}$$

$$= | P(\omega) | ^2[(2N+1) +$$

$$+ | E\{e^{j\omega T_s c_n}\} | ^2 | E\{e^{j\omega\tau_n}\} | ^2 \sum_{m\neq n} e^{j\omega QT_s(m-n)}]$$

$$= | P(\omega) | ^2[(2N+1) (1 - | C(\omega) | ^2 | M_\tau(\omega) | ^2)$$

$$+ | C(\omega) | ^2 | M_\tau(\omega) | ^2 | \sum_{n=-N}^{N} e^{-j\omega QT_s n} | ^2]. \tag{A.2}$$

The power spectrum (3.5) can be obtained by taking the the limit of (A.2) as $T\rightarrow\infty$, therefore,

$$S(\omega) = | P(\omega) | ^2[\frac{1}{QT_s}(1- | C(\omega) | ^2 | M_\tau(\omega) | ^2) +$$

$$+ | C(\omega) | ^2 | M_\tau(\omega) | ^2 \lim_{T\rightarrow\infty} \frac{1}{2T} | \sum_{n=-N}^{N} e^{-j\omega QT_s n} | ^2]. \tag{A.3}$$

Since $\sum_{n=-\infty}^{\infty} e^{-jxn} = 2\pi \sum_{k=-\infty}^{\infty} \delta(x-2\pi k)$, and $\delta(ax)=\frac{1}{|a|}\delta(x)$, then,

$$\lim_{T\rightarrow\infty} \frac{1}{2T} | \sum_{n=-N}^{N} e^{-j\omega QT_s n} | ^2 = \lim_{T\rightarrow\infty} \frac{1}{2T}[\frac{2\pi}{QT_s} \sum_{n=-\infty}^{\infty} \delta(\omega-2\pi n/QT_s)]^2$$

$$= \frac{4\pi^2}{(QT_s)^2} \sum_{n=-\infty}^{\infty} \lim_{T\rightarrow\infty} \frac{1}{2T}\delta^2(\omega-2\pi n/QT_s). \tag{A.4}$$

Using the relationship that $\delta(\omega)=\frac{1}{2\pi}\lim_{T\rightarrow\infty} 2T\frac{\sin(\omega T)}{\omega T}$, each term in the sum of (A.5) reduces to

$$\lim_{T\rightarrow\infty} \frac{1}{2T}\delta^2(\omega-2\pi n/QT_s)= \lim_{T\rightarrow\infty} \frac{1}{2T}\cdot\frac{1}{2\pi}2T\frac{\sin(\omega-2\pi n/QT_s)T}{(\omega-2\pi n/QT_s)T}\cdot\delta(\omega-2\pi n/QT_s)$$

$$= \frac{1}{2\pi}\delta(\omega-2\pi n/QT_s). \tag{A.5}$$

According to (3.9),

$$| C(\omega) | = \frac{1}{Q} | \frac{1 - e^{j\omega T_s Q}}{1 - e^{j\omega T_s}} | = \frac{1}{Q} | \frac{\sin(\omega T_s Q/2)}{\sin(\omega T_s/2)} | , \tag{A.6}$$

therefore, $| C(2\pi n/QT_s) | =1$ if $n=kQ$ for any integer k, and $| C(2\pi n/QT_s) | =0$ otherwise. Substituting (A.4), (A.5), and (A.6) into (A.3), the power spectrum of PPM signal is given by

$$S(\omega) = | P(\omega) |^2 [\frac{1}{QT_s}(1- | C(\omega) |^2 | M_r(\omega) |^2) +$$

$$+ \frac{2\pi}{(QT_s)^2} | M_r(\omega) |^2 \sum_{k=-\infty}^{\infty} \delta(\omega-2\pi k/T_s)]. \tag{A.7}$$

Appendix B

Variance of Threshold Crossing Times at $B\Delta T_c=0$

The impulse response of the low pass filter (3.26) and its derivative at time $t=T_c-t_0$ can be rewritten by substituting the new variable $\Delta T_c \equiv T_c-(t_0+t_d)$, as,

$$h(T_c-t_0) = 2B\frac{\sin 2\pi B\Delta T_c}{2\pi B\Delta T_c} \tag{B.1}$$

$$\frac{d}{dt}h(T_c-t_0) = 2B\frac{2\pi B\Delta T_c \cos 2\pi B\Delta T_c - \sin 2\pi B\Delta T_c}{2\pi B\Delta T_c^2}. \tag{B.2}$$

Next,

$$\int_0^{T_c-t_0} h^2(u)du = \int_{-t_d}^{T_c-t_0-t_d} h^2(v+t_d)dv \approx \int_{-\infty}^{\Delta T_c} (2B\frac{\sin 2\pi Bv}{2\pi Bv})^2 dv$$

$$= B + \frac{2B}{\pi}\int_0^{2\pi B\Delta T_c} (\frac{\sin x}{x})^2 dx, \tag{B.3}$$

where the relationship $\int_{-\infty}^{0} (\frac{\sin x}{x})^2 dx = \frac{\pi}{2}$ has been used. When $B\Delta T_c \to 0$, equation (B.1), (B.2), and (B.3) reduce to $h(T_c-t_0) = 2B$, $\frac{d}{dt}h(T_c-t_0) = 0$, and

$\int_0^{T_c - t_0} h^2(u)du = B$. Substituting these into (3.24), the variance of threshold crossing time at $B\Delta T_c = 0$ becomes

$$\sigma_\tau^2 = \frac{FG^2\lambda_1 + \dfrac{4kT_r}{Re^2}}{4BG^2\lambda_1^2}. \tag{B.4}$$

References

[1] D. L. Snyder, *Random Point Processes,* New York: John Wiley and Sons, Inc., 1975.

[2] R. Gagliardi and S. Karp, *Optical Communication,* ch. 8, 9 & 10, John Wiley and Sons, Inc., New York, 1976.

[3] J. B. Abshire, "Performance of OOK and low-order PPM modulations in optical communications when using APD-based receivers," *IEEE Trans. Commun.,* vol. COM-32, no. 10, pp. 1140-1143, Oct. 1984.

[4] T. V. Muoi, "Receiver design for digital optic transmission system using Manchester (biphase) coding," *IEEE Trans. Commun.,* vol. COM-31, no. 5, pp. 608-619, May 1983.

[5] X. Sun, F. Davidson and J. B. Abshire, "Performance measurements of a diode laser optical communications link with Q=4 PPM signaling," *Optical Technologies for Space Communication Systems,* K. Bhasin and G. A. Koepf ed., proc. SPIE 756, pp. 50-53, 1987.

[6] F. Davidson and X. Sun, "Gaussian approximation versus nearly exact performance analysis of optical communication systems with PPM signaling and APD receivers," to appear on *IEEE Trans. Commun.*

[7] C. N. Georghiades, "Optimum joint slot and symbol synchronization for the optical PPM channel," *IEEE Trans. Commun.,* vol. COM-35, no. 6, pp. 632-636, June 1987.

[8] G. L. Lui and H. H. Tan, "On joint symbol and frame synchronization for direct-detection optical communication systems," *IEEE Trans. Commun.,* vol. COM-35, no. 2, pp. 250-255, Feb. 1987.

[9] G. L. Lui and H. H. Tan, "Frame synchronization for direct-detection optical communication systems," *IEEE Trans. Commun.*, vol. COM-34, no. 3, pp. 227-234, Mar. 1986.

[10] R. J. McIntyre, "The distribution of gains in uniformly multiplying avalanche photodiodes: Theory," *IEEE Trans. Electron Devices,* vol. ED-19, pp. 703-713, June 1972.

[11] J. Conradi, "The distribution of gains in uniformly multiplying avalanche phótodiodes: Experimental," *IEEE Trans. Electron Devices,* vol. ED-19, pp. 713-718, June 1972.

[12] F. Andreucci and U. Mengali, "Timing extraction in optical transmissions," *Optical and Quantum Electronics*, vol. 10, pp. 455-458, 1978.

[13] R. L. Rosenberg and et al, "Optical fiber repeatered transmission systems utilizing SAW filters," *IEEE Trans. Sonics and Ultrasonics*, vol. 30, no. 3, pp. 119-126, May 1983.

[14] U. Mengali and E. Pezzani, "Tracking properties of phase locked loops in optical communication systems," *IEEE Trans. Commun.*, vol. COM-26, no. 12, pp. 1811-1818, Dec. 1978.

[15] C. C. Chen and C. S. Gardner, "Performance of PLL synchronized optical PPM communication systems," *IEEE Trans. Commun.*, vol. COM-34, no. 10, pp. 988-994, Oct. 1986.

[16] G. Ling and R. Gagliardi, "Slot synchronization in optical PPM communications," *IEEE Trans. Commun.*, vol. COM-34, no. 12, pp. 1202-1208, Dec. 1986.

[17] D. Datta and R. Gangopadhyay, "Simulation studies on nonlinear bit synchronizers in APD-based optical receivers," *IEEE Trans. Commun.*, vol. COM-35, no. 9, pp. 909-917, Sept. 1987.

[18] S. D. Personick, "Design of Repeaters for Fiber Systems," in *Fundamentals of Optical Fiber Communications*, ch. 6, M. K. Barnoski ed., Academic Press, Inc., New York, 1976, p. 199.

[19] L. E. Franks, "Carrier and bit synchronization in data communication — a tutorial review," *IEEE Trans. Commun.*, vol. COM-28, no. 8, pp. 1107-1121, Aug. 1980.

[20] F. M. Gardner, *Phaselock Techniques*, ch. 11, New York: John Wiley and Sons, Inc., 1979.

[21] W. R. Bennett, "Statistics of regenerative digital transmission," *Bell sys. Tech. J.*, vol. 37, pp. 1501-1542, Nov. 1958.

[22] R.G. Smith and S. D. Personick, "Receiver design for optical fiber communication systems," in *Semiconductor Devices for Optical Communication*, H. Kressel ed., ch. 4, New York: Spring-Verlag, 1980.

[23] A. J. Viterbi, *Principles of coherent communication*, New York: McGraw-Hill, 1966, p. 226.

Figure Captions

Fig. 1. Block diagram of a slot clock recovery system with a transition detector.

Fig. 2. Normalized rms threshold crossing time, σ_τ/T_s, vs. normalized mean threshold crossing time, $B\Delta T_c$.

Fig. 3. Block diagram of the matched filter.

Fig. 4. The output of the matched filter shown in Fig. 3 in response to a rectangular input pulse. The dotted line corresponds to the output of an ideal matched filter.

Fig. 5. Block diagram of the rms phase error detector.

Fig. 6. Normalized rms phase error of the recovered slot clock, $\sigma_\phi/2\pi$, vs. average number of photons per bit. The curves are obtained by numerical evaluations of (3.28). The squares and triangles represent the experimental measurements.

Fig. 7. Probability of bit error vs. average number of photons per bit when the slot clock regenerated by a PLL (B_L=1 KHz) was used. The background noise intensity was n_b=0.0122/slot. The solid curve is obtained as in [6] assuming perfect slot clock. The dashed curve represent the upper bound given by (4.5). The small crosses and triangles represent the experimental data.

Fig. 8. Same as Fig. 7, but with the slot clock regenerated by a narrowband filter (B_L=9.5 KHz).

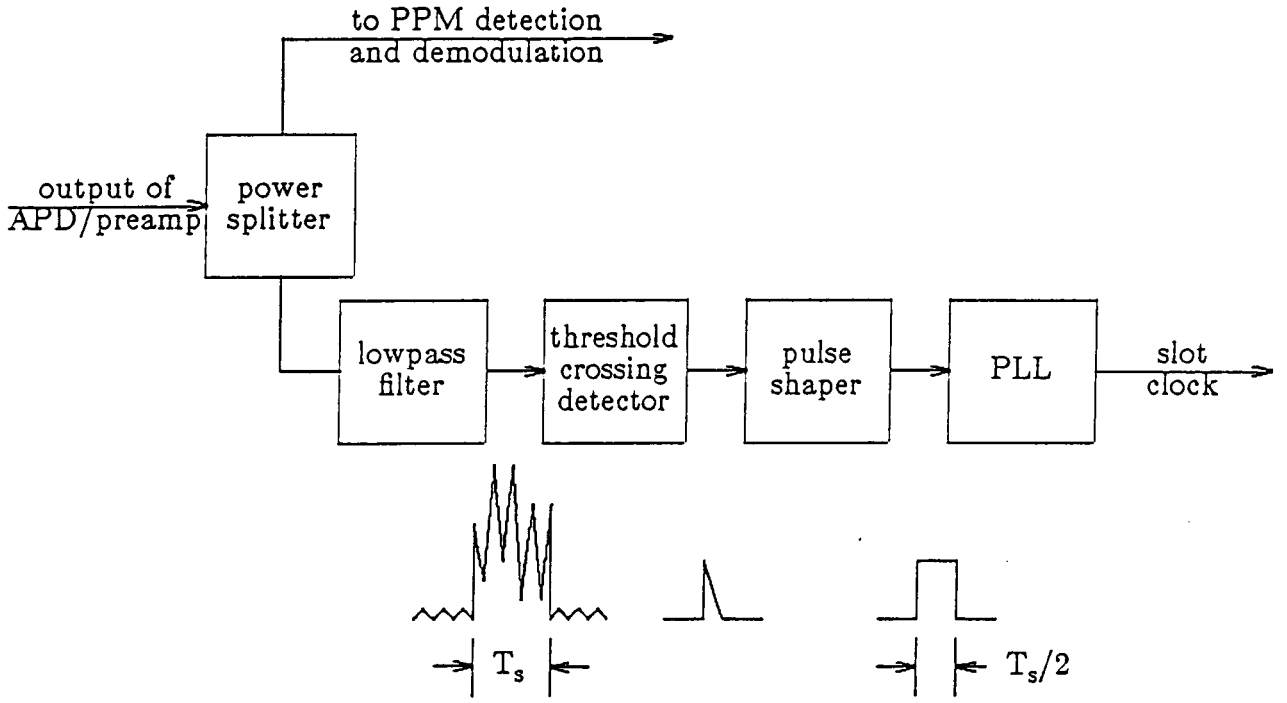
to PPM detection
and demodulation
output of
APD/preamp
power
splitter
lowpass
filter
threshold
crossing
detector
pulse
shaper
PLL
slot
clock
T_s
$T_s/2$

Fig 1

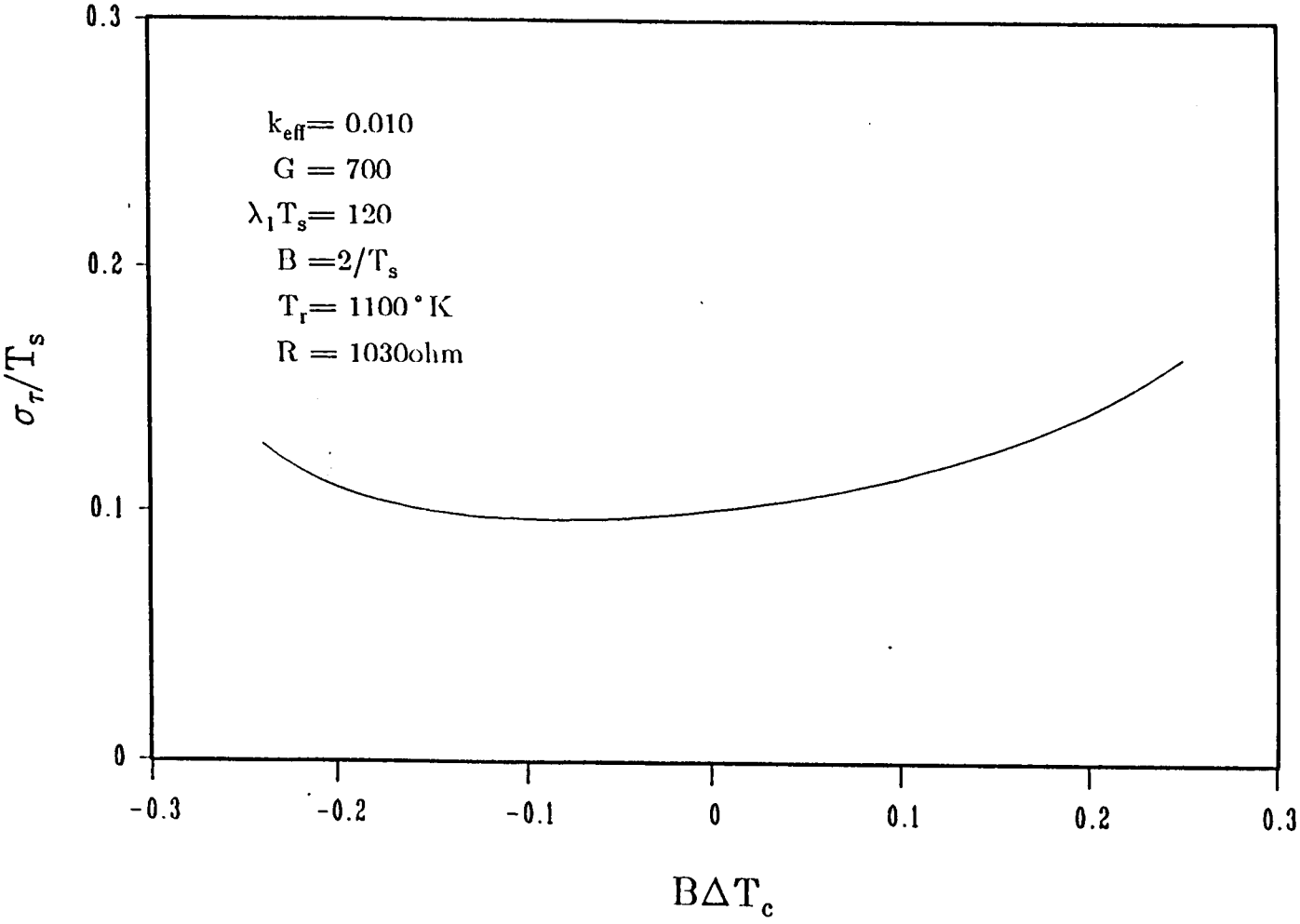
0.3
0.2
0.1
0
k_{eff}= 0.010
G = 700
$\lambda_1 T_s$= 120
B =2/T_s
T_r= 1100 °K
R = 1030ohm
σ_π/T_s
-0.3
-0.2
-0.1
0
0.1
0.2
0.3
$B\Delta T_c$

Fig 2

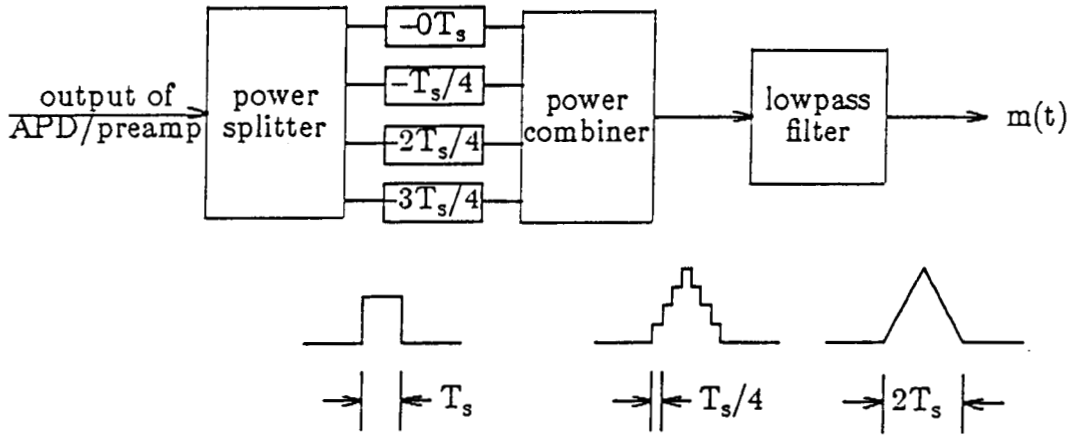
output of
APD/preamp
power
splitter
-0T_s
-T_s/4
-2T_s/4
-3T_s/4
power
combiner
lowpass
filter
m(t)
T_s
T_s/4
2T_s

Fig 3

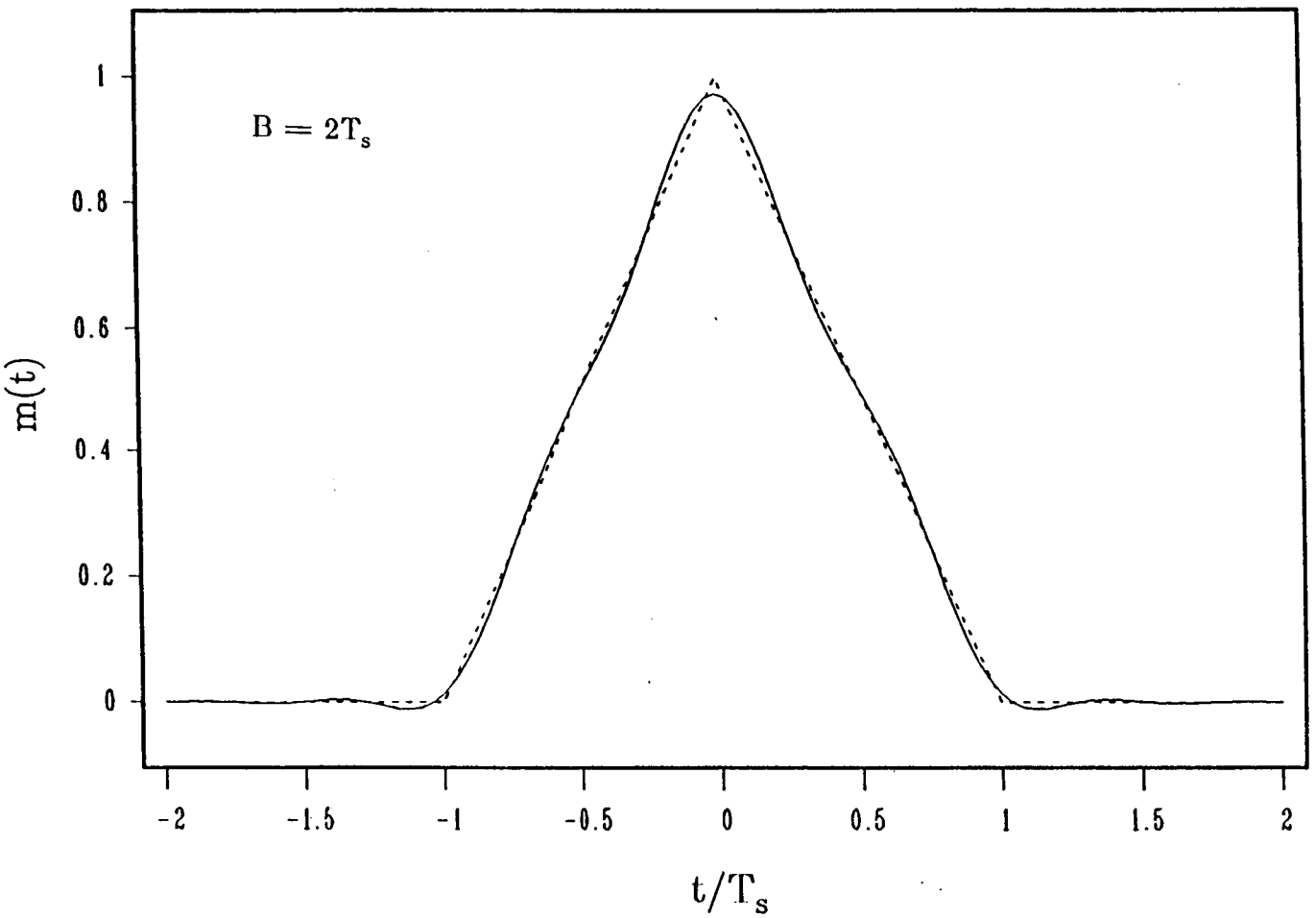

Fig 4

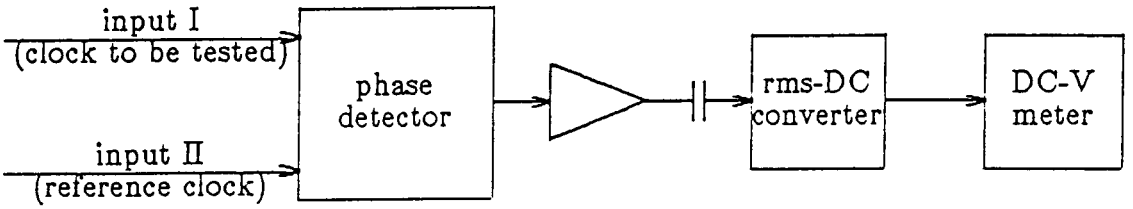
input I
(clock to be tested)
input II
(reference clock)
phase
detector
rms-DC
converter
DC-V
meter

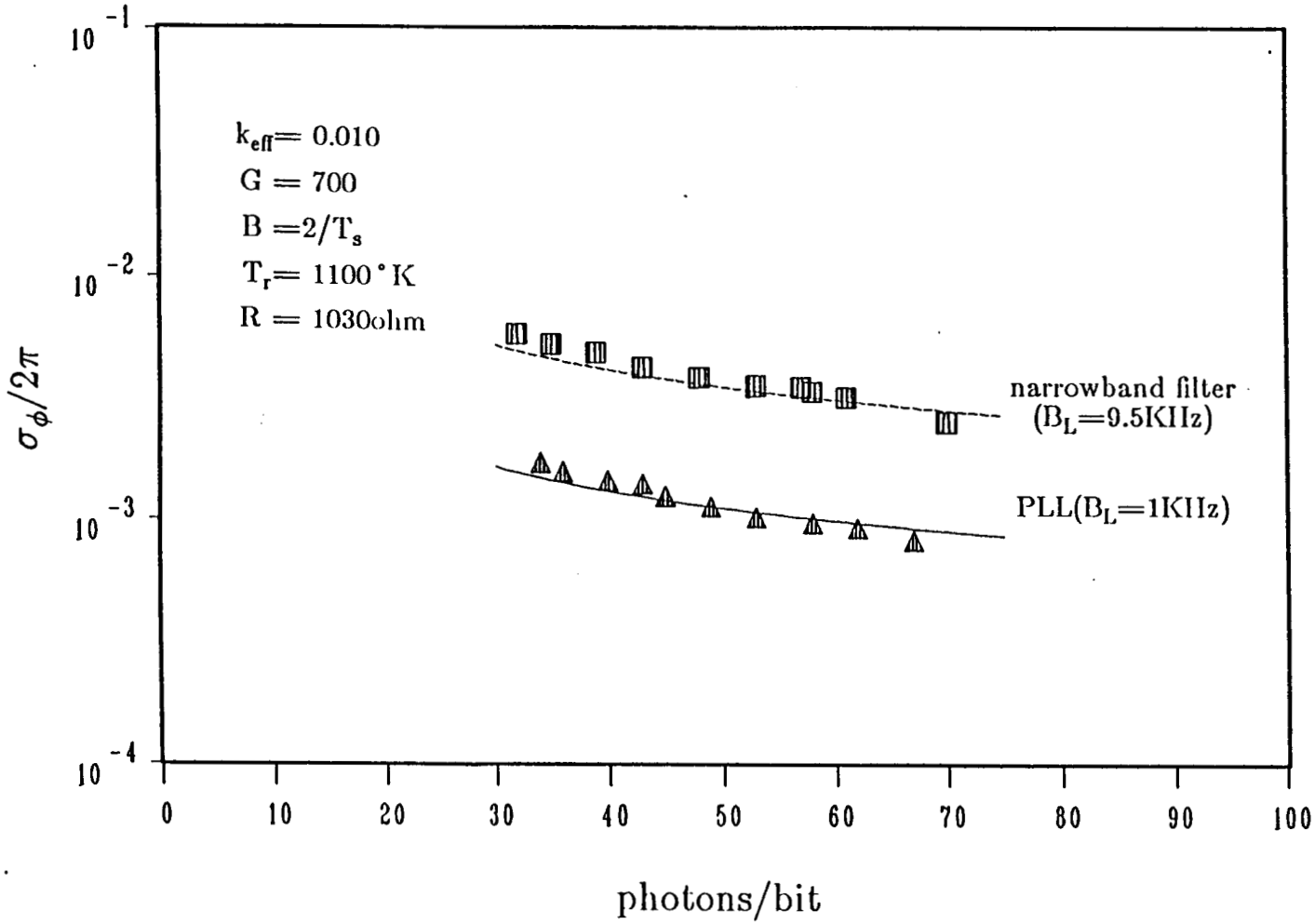
10^{-1}
10^{-2}
10^{-3}
10^{-4}
$\sigma_\phi/2\pi$
k_{eff}= 0.010
G = 700
B =2/T_s
T_r= 1100 °K
R = 1030ohm
narrowband filter
(B_L=9.5KHz)
PLL(B_L=1KHz)
0
10
20
30
40
50
60
70
80
90
100
photons/bit

Fig 6

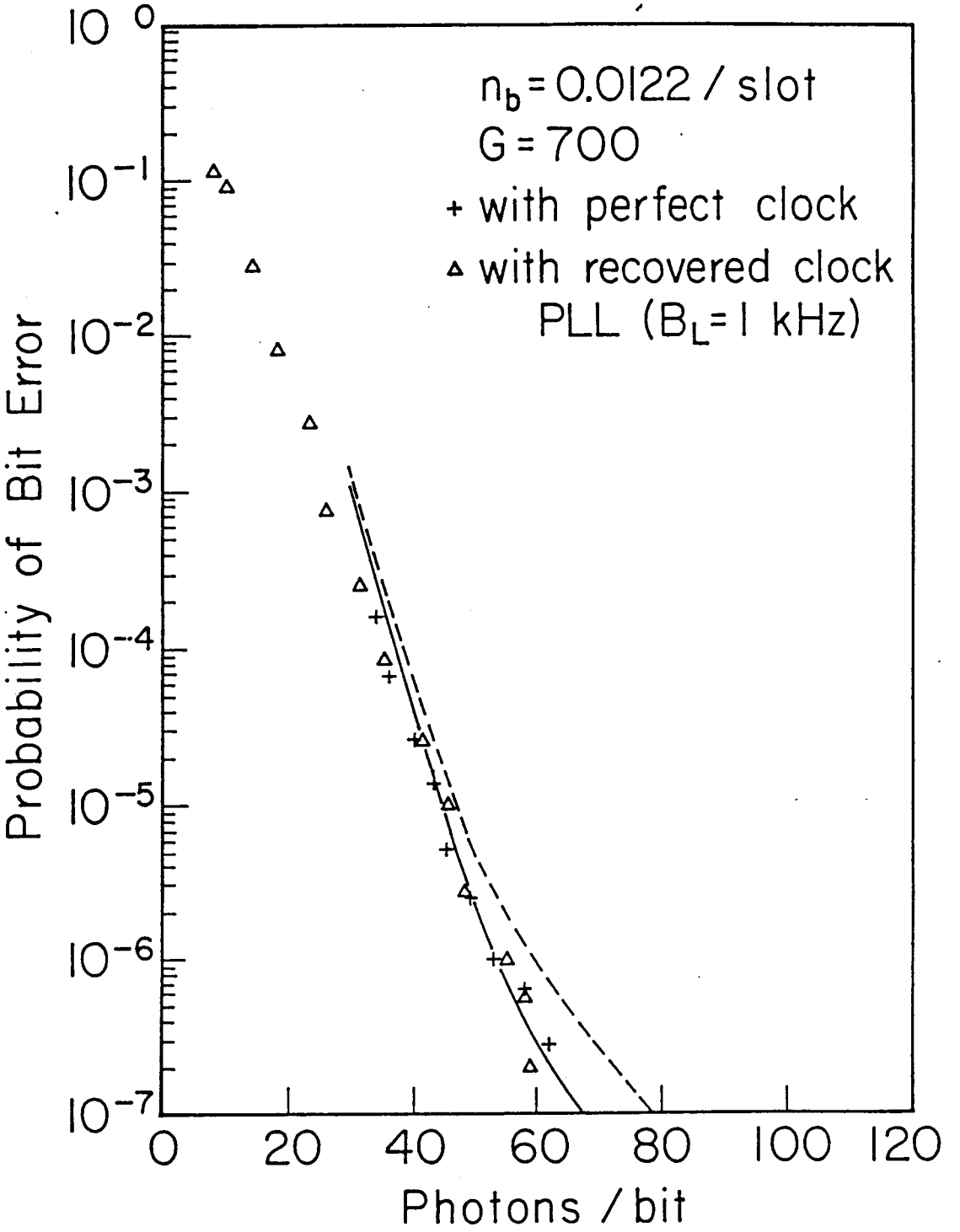
n_b = 0.0122 / slot
G = 700
+ with perfect clock
Δ with recovered clock
PLL (B_L = 1 kHz)
Probability of Bit Error
10^{0}
10^{-1}
10^{-2}
10^{-3}
10^{-4}
10^{-5}
10^{-6}
10^{-7}
0
20
40
60
80
100
120
Photons / bit

Fig. 7

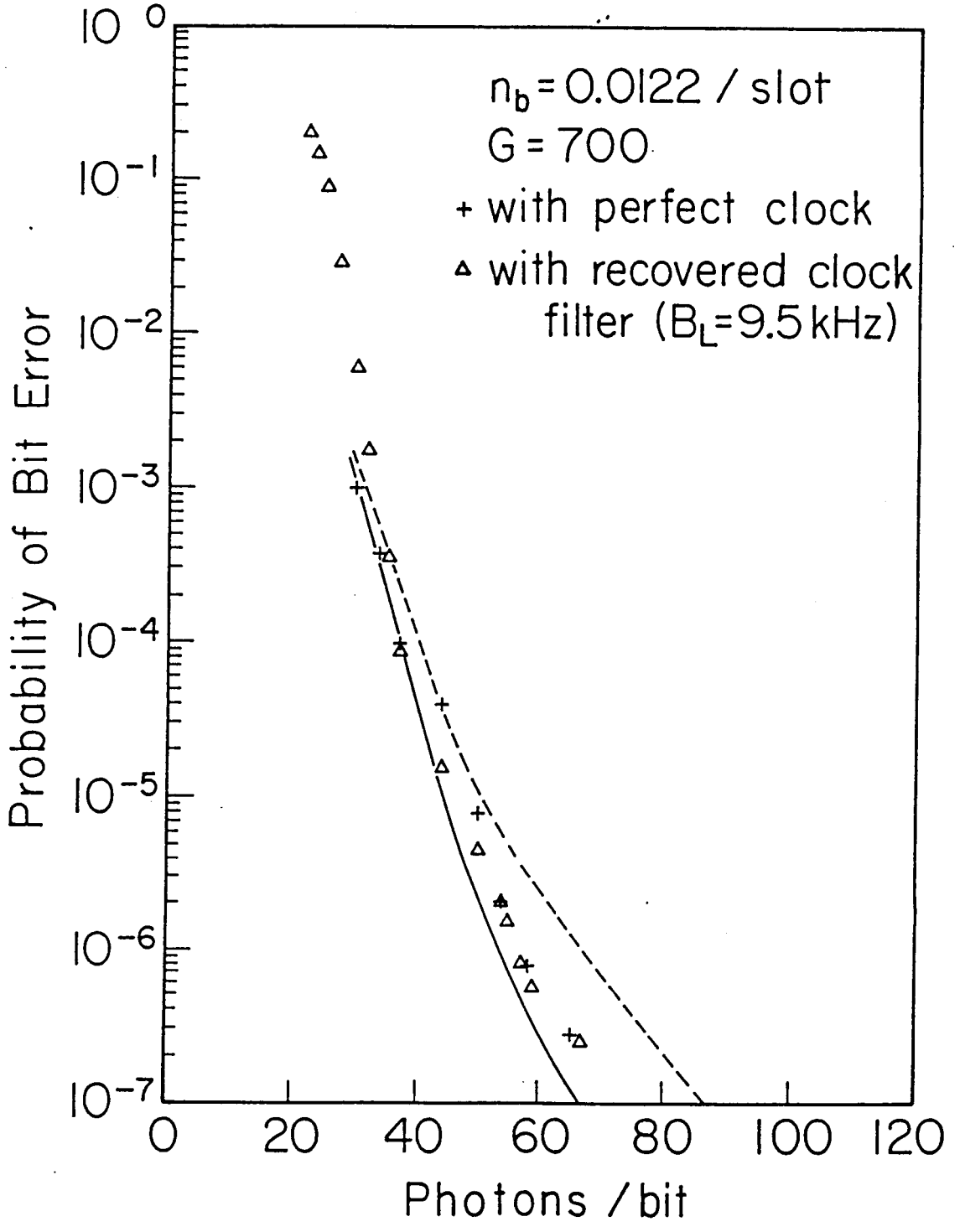
n_b = 0.0122 / slot
G = 700
+ with perfect clock
Δ with recovered clock
filter (B_L=9.5 kHz)
Probability of Bit Error
10^{0}
10^{-1}
10^{-2}
10^{-3}
10^{-4}
10^{-5}
10^{-6}
10^{-7}
0
20
40
60
80
100
120
Photons / bit

Fig 8